Performance of DS-UWB Multiple-Access Systems With Diversity Reception in Dense Multipath Environments

Sheu-Sheu Tan, *Student Member, IEEE*, Arumugam Nallanathan, *Senior Member, IEEE*, and Balakrishan Kannan, *Member, IEEE*

***Abstract*—Ultrawideband (UWB) technology is characterized by transmitting extremely short duration radio impulses. To improve its multiple-access capability, the UWB technology can be combined with traditional spread-spectrum techniques. This paper demonstrates the influence of spatial and temporal diversities on the performance of direct-sequence (DS) UWB multiple-access systems in dense multipath environments. Numerical results show that the bit error rate performance of the DS-UWB system can be improved significantly by increasing the number of antenna array elements and/or by adding more multipaths coherently at the receiver. Furthermore, this paper studies the impact of array geometry on system performance and shows that a rectangular array can capture more energy and thus can offer better performance than a uniform linear array.**

***Index Terms*—Antenna array, direct sequence (DS), multiple access, ultrawideband (UWB).**

I. Introduction

Ultrawideband (UWB) technology has attracted considerable interest from research and standardization communities due to its promising ability to provide high data rate at low cost with relatively low power consumption. UWB radio signals employ the transmission of very short impulses whose spectrum extends across a wide range of frequencies [1]. To improve the multiple-access capability, the UWB impulse radio technology can be combined with traditional spread-spectrum (SS) techniques. Most of the research on multiple-access UWB has focused on time hopping (TH) SS using pulse-position-modulated (PPM) signals [2]. The direct-sequence (DS) SS technique is a well-known and powerful multiple-access technology. Antipodal signaling, such as binary phase shift keying (BPSK), can be employed with DS-UWB and is supported by the current technology [3]–[6]. In DS-UWB, multiple pulses are transmitted during one data symbol duration using bipolar modulation based upon a certain spreading sequence. This method has many attractive properties, including low peak-to-average power ratio and robustness to multiuser interference.

One of the potential benefits of UWB radio is its multipath resolution. The multipath components that might not be resolved as distinct arrivals in narrowband systems can be separately identified in UWB systems. Consequently, the Rake receiver can be used advantageously to reap the benefits of multipath diversity in UWB systems. The analysis on Rake-type receivers for the UWB system in dense multipath environments is discussed in [7]–[9].

Much attention has been paid on the design and implementation of antenna arrays for future wireless communication systems [10], [11]. The motivation is that the antenna array is a promising approach that can significantly improve the capacity, coverage, and quality in wireless networks by exploiting the spatial dimension. However, application of space–time array processing in UWB systems is still new, and not much research works have been done in this area. Applications of antenna diversity in impulse radio to improve the bit error rate (BER) performance are reported in [12] and [13]. It is shown in these papers that the antenna array can be used to exploit the spatial diversity in conjunction with the path diversity provided by the Rake receiver to capture the energy from different multipath components that are separated in space and time in a way to improve the performance of the impulse radio system. The principles of space–time array processing for impulse radio are discussed in [14], where the advantages of antenna arrays in a UWB system are described.

In this paper, the BER performance of the binary modulated DS-UWB system with antenna array in the presence of multipaths and multiple-access interference (MAI) is presented. Specially, uniform rectangular and linear arrays with Selective Rake (SRake) are employed at the receiver to obtain the spatial and temporal diversities. Particular attention is given to the effects of the number of employed antenna elements and the number of selected multipaths on BER performance.

This paper is organized as follows: The system model is introduced in Section II. Section III describes the channel model. DS-UWB receiver processing and BER analysis are presented in Sections IV and V, respectively. The numerical results are given in Section VI. Finally, conclusions are drawn in Section VII.

II. System Model

A. DS-UWB Signal Model

We consider a DS-UWB system with N_u asynchronous users. Each user has a user-specific pseudonoise (PN) sequence

Manuscript received August 17, 2004; revised May 27, 2005 and August 31, 2005. The review of this paper was coordinated by Dr. O. C. Ugweje.

S.-S. Tan and A. Nallanathan are with the Department of Electrical and Computer Engineering, National University of Singapore, Singapore 119260 (e-mail: engp2444@nus.edu.sg; elena@nus.edu.sg).

B. Kannan is with the School of Electrical Engineering and Telecommunications, University of New South Wales, Sydney, NSW 2052 Australia.

Digital Object Identifier 10.1109/TVT.2006.877694

with N_s chips per data symbol period T_b such that $T_b = N_s T_c$, where N_s is the processing gain, and T_c is the chip duration. A typical DS-UWB signal of the uth user can be expressed as

$$s^{(u)}(t) = \sum_{i=-\infty}^{\infty} q_i(t) \tag{1}$$

where $q_i(t)$ represents the signal for the ith data symbol and is given by

$$q_i(t) = \sum_{j=iN_s}^{(i+1)N_s-1} b_i^{(u)} a_j^{(u)} w(t - iT_b - jT_c) \tag{2}$$

where $w(t)$ represents the received monocycle waveform at the output of the receiver, and $\{b_i^{(u)}\}$ and $\{a_j^{(u)}\}$ denote the data symbols and the spreading chips for the[1] uth user, respectively. The monocycle waveform $w(t)$ is modeled as a second-derivative Gaussian pulse and is given by

$$w(t) = \sqrt{\frac{8}{3 \times \tau_m \times N_s}} \times \left(\left[1 - 4\pi \left(\frac{t - t_d}{\tau_m} \right)^2 \right] \exp\left[-2\pi \left(\frac{t - t_d}{\tau_m} \right)^2 \right] \right) \tag{3}$$

where t_d corresponds to the location of the pulse center in time, and τ_m is the parameter that determines the temporal width of the pulse. The square root term in (3) is the normalization factor that ensures that the total energy in one symbol (N_s pulses) is equal to 1. In this paper, the chip duration T_c is equal to the duration of a monocycle waveform.

B. Antenna Array Geometry and Its Parameters

In this paper, we consider uniform rectangular ($R_x = M \times N$) and linear ($R_x = M \times 1$) arrays. The delay and sum beamformer is used to process the received signals at the array elements. The beamformer output for an array steered toward an azimuth angle of ϕ and an elevation angle of θ on the incidence of a plane wave from an azimuth angle of ϕ_0 and an elevation angle of θ_0 is given by [15]

$$B(\phi, \theta, t) = \sum_{m=0}^{M-1} \sum_{n=0}^{N-1} a_{m,n}(\phi, \theta) \times w(t - \tau_{m,n}) \tag{4}$$

$$\tau_{m,n} = \left[(M_c m) \frac{d_x}{c} (\kappa - \kappa_0) \right] + \left[(n - N_c) \frac{d_y}{c} (\upsilon - \upsilon_0) \right] \tag{5}$$

where $\kappa = \sin\phi \sin\theta$, $\kappa_0 = \sin\phi_0 \sin\theta_0$, $\upsilon = \cos\phi \sin\theta$, $\upsilon_0 = \cos\phi_0 \sin\theta_0$, and c is the speed of light. The spacings between antenna elements in x and y directions are denoted by d_x and d_y, respectively. The antenna elements are equally spaced. The coordinate of the reference element is (M_c, N_c). The pattern of the (m, n)th antenna element is denoted by $a_{m,n}(\phi, \theta)$. The time delay of the received signal at the (m, n)th element is given by $\tau_{m,n}$, which is measured with respect to the reference element. Each element is assumed to have an isotropic pattern, and thus, $a_{m,n}(\phi, \theta) = 1/(4\pi)$.

III. Channel Model

The channel model used in this paper is similar to the one described in [16] and [17], which is based on the Saleh–Valenzuela (S–V) model [18] with slight modifications. The amplitude statistics in the original S–V model were found to best fit the Rayleigh distribution. However, the measurements in UWB channels indicate that the amplitudes do not follow a Rayleigh distribution. A lognormal distribution is recommended in [16] and [17], rather than a Rayleigh distribution, for the multipath gain magnitude.

The S–V channel model is characterized by the clustering phenomenon of rays. The magnitudes of the clusters and rays attenuate exponentially with time, which are characterized by the cluster decay factor (Γ) and the ray decay factor (γ), respectively. Typically, $\Gamma > \gamma$, hence the rays within different clusters do not overlap. We consider a constant cluster arrival rate (Λ) and ray arrival rate (λ), where $\lambda > \Lambda$ with deterministic cluster and ray arrival time. Each ray within each cluster has an associated time delay, an azimuth angle ϕ, and an elevation angle θ. As in [16] and [17], independent fading is assumed for each cluster and for each ray within the cluster. In addition, we also assume independent fading for each antenna element.

We denote the arrival time of the qth cluster by τ_q, where $q = 0, 1, 2, \ldots, Q - 1$, and the arrival time of the kth ray measured from the beginning of the qth cluster by $\tau_{k,q}$, where $k = 0, 1, 2, \ldots, K - 1$. The total number of multipaths is $L_{\text{total}} = Q \times K$. The channel impulse response can be written as

$$\begin{aligned} h(t) &= \sum_{m=0}^{M-1} \sum_{n=0}^{N-1} \sum_{q=0}^{Q-1} \sum_{k=0}^{K-1} \alpha_{k,q,m,n} \delta(t - \tau_{m,n} - \tau_q - \tau_{q,k}) \\ &= \sum_{m=0}^{M-1} \sum_{n=0}^{N-1} \sum_{q=0}^{Q-1} \sum_{k=0}^{K-1} \alpha_{k,q,m,n} \delta\left(t - \tau_{k,q,m,n}\right) \\ &= \sum_{m=0}^{M-1} \sum_{n=0}^{N-1} \sum_{l=0}^{L_{\text{total}}-1} \alpha_{l,m,n} \delta\left(t - \tau_{l,m,n}\right) \end{aligned} \tag{6}$$

where $\alpha_{k,q,m,n} \in \Re$, $\tau_{k,q,m,n} = \tau_{m,n} + \tau_q + \tau_{k,q}$, and $\delta(t)$ is the Dirac delta function. The random variable $\alpha_{k,q,m,n}$ represents the gain coefficient of the kth ray within the qth cluster at the (m, n)th antenna element. The parameter $\tau_{k,q,m,n}$ is the time delay of the kth ray of the qth cluster associated with the (m, n)th antenna element with respect to the first ray of the first cluster at the reference antenna element.

The magnitudes of the channel gain follow a lognormal distribution [16], where

$$\alpha_{k,q,m,n} = \varsigma_{k,q,m,n} \xi_{q,m,n} \beta_{k,q,m,n} \tag{7}$$

$$20 \log_{10}(\xi_{q,m,n} \beta_{k,q,m,n}) \propto \text{Normal}\left(\mu_{k,q,m,n}, \sigma_1^2 + \sigma_2^2\right). \tag{8}$$

[1]Superscript u refers to the uth user.

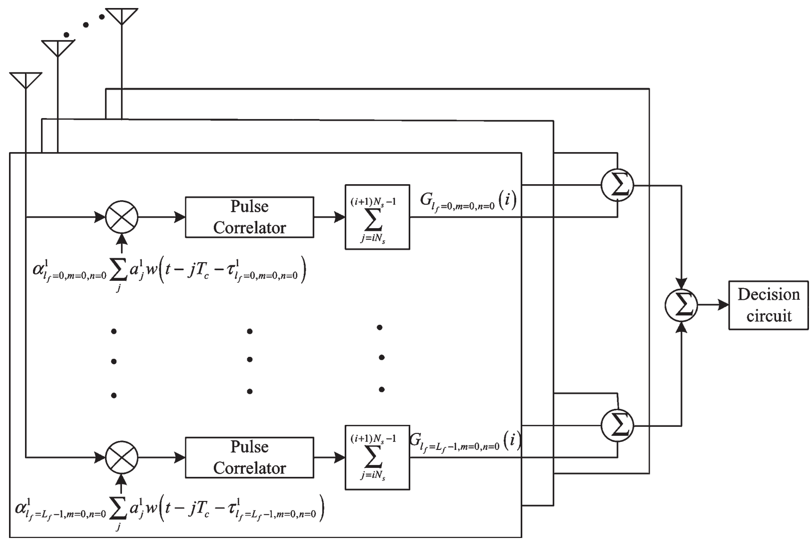

Fig. 1. Receiver structure with $(M \times N)$ antenna array.

In (7), $\xi_{q,m,n}$ corresponds to the fading associated with the qth cluster of the (m,n)th antenna element, $\beta_{k,q,m,n}$ reflects the fading associated with the kth ray in the qth cluster of the (m,n)th antenna element, and $\varsigma_{k,q,m,n}$ can be $+/-$ with equal probability. The log value of each channel gain follows a normal distribution with mean $\mu_{k,q,m,n}$ and variance $\sigma_1^2+\sigma_2^2$, where σ_1^2 is the variance of the cluster lognormal fading term in decibels and σ_2^2 is the variance of the ray lognormal fading term in decibels. The normalized mean square value of $\alpha_{k,q,m,n}$, $\mathrm{E}[\alpha_{k,q,m,n}^2]$ is defined as

$$\mathrm{E}\left[\alpha_{k,q,m,n}^2\right] = \Omega_0 e^{-\tau_{q,m,n}/\Gamma} e^{-\tau_{k,q,m,n}/\gamma} \tag{9}$$

where $\Omega_0 = (\alpha_{0,0,M_c,N_c}^2)/(\sum_{q=0}^{Q-1}\sum_{k=0}^{K-1}\alpha_{k,q,M_c,N_c}^2)$ is the average power gain of the first ray within the first cluster of the reference antenna element (M_c,N_c), which is normalized by the total power of the reference antenna element. Thus, the power of each ray within each cluster at every antenna element is normalized by the total power of the reference antenna element. The term $\mu_{k,q,m,n}$ in (8) is thus given by

$$\mu_{k,q,m,n} = \frac{10\ln(\Omega_0) - 10\tau_{q,m,n} - 10\tau_{k,q,m,n}}{\ln(10)} - \frac{\left(\sigma_1^2+\sigma_2^2\right)\ln(10)}{20}. \tag{10}$$

In order to simplify the notations, we index the multipaths at the (m,n)th element in ascending order such that the path index l takes a value in $\{0,\ldots,QK-1\}$ [see (6)], where $l = qK + k$. In (6), $\alpha_{l,m,n}$ is the channel gain of the lth path at the (m,n)th antenna element, and $\tau_{l,m,n}$ is the corresponding time delay.

IV. DS-UWB Receiver Processing

Fig. 1 shows the receiver structure. Each and every element of the $(M \times N)$ antenna array is equipped with SRake with L_f Rake fingers. Space–time correlators process the received signals that are separated in space and time. We use the maximal ratio combining (MRC) scheme to combine the signals from the Rake fingers.

Without loss of generality, we assume that the receiver is perfectly synchronized to the spreading sequence of the desired user (user 1), the delays and channel coefficients of the selected paths are known at the receiver, and the receiver selects $L_f^{u=1}$ dominant paths of user 1. The received signal can be written as

$$r(t) = \sum_{m=0}^{M-1}\sum_{n=0}^{N-1}\sum_{l_f=0}^{L_f^1-1} \alpha_{l_f,m,n}^1 s^1\left(t-\tau_{l_f,m,n}^1\right) + n_{\mathrm{si}}(t) + n_{\mathrm{mai}}(t) + \eta'(t) \tag{11}$$

where $n_{\mathrm{si}}(t) = \sum_{m=0}^{M-1}\sum_{n=0}^{N-1}\sum_{l=L_f^1}^{L_{\mathrm{total}}^1-1}\alpha_{l,m,n}^1 s^1(t-\tau_{l,m,n}^1)$ is the interference from the nonselected paths of user 1 [self-interference (SI)], $n_{\mathrm{mai}}(t) = \sum_{u=2}^{N_u}\sum_{m=0}^{M-1}\sum_{n=0}^{N-1}\sum_{l=0}^{L_{\mathrm{total}}^u-1} \times \alpha_{l,m,n}^u s^u(t-\tau_{l,m,n}^u)$ is the interference from undesired users (MAI), and $\eta'(t) = \sum_{m=0}^{M-1}\sum_{n=0}^{N-1}\eta'_{m,n}(t)$ is the noise term. Here, $\eta'_{m,n}(t)$ is the additive white Gaussian noise (AWGN) noise at the (m,n)th element with double-sided power spectral density of $N_0/2$. In (11), $\alpha_{l,m,n}^u$ is the channel gain of the lth path at the (m,n)th antenna element for the uth user, and $\tau_{l,m,n}^u$ is the time delay of the lth path at the (m,n)th element for the user u. Without lost of generality, we assume $\tau_{0,M_c,N_c}^1 = 0$.

The received signal is correlated with the correspondent template waveform at each finger of every antenna element, followed by sampling and summation as shown in Fig. 1. At each finger, one path is selected for the MRC, and the rest of the unselected paths are treated as SI or noise.

The correlator output at the l_fth finger of the (m,n)th element during the ith symbol period $G_{l_f,m,n}(i)$ is given as shown in (12) at the bottom of the next page.

In (12), $s_{l_f,m,n}$ and $N_{l_f,m,n}$ are the desired and undesired signals at the output of the l_fth rake finger of the (m,n)th antenna element, respectively. The terms $Ns_{l_f,m,n}$, $Nm_{l_f,m,n}$, and $Na_{l_f,m,n}$, respectively, denote the undesired contributions from SI, MAI, and AWGN noise to the selected l_fth path at the (m,n)th array element.

Now, the test statistic for the ith transmitted symbol can be written as

$$\begin{aligned} G(i) &= \sum_{m=0}^{M-1}\sum_{n=0}^{N-1}\sum_{l_f=0}^{L_f^1-1} G_{l_f,m,n}(i) \\ &= \underbrace{\sum_{m=0}^{M-1}\sum_{n=0}^{N-1}\sum_{l_f=0}^{L_f^1-1} s_{l_f,m,n}}_{S_T} + \underbrace{\sum_{m=0}^{M-1}\sum_{n=0}^{N-1}\sum_{l_f=0}^{L_f^1-1} N_{l_f,m,n}}_{N_T} \end{aligned} \tag{13}$$

where the total desired signal output is denoted as s_T, which is the sum of desired signal outputs $(s_{l_f,m,n})$ from all selected fingers of all antenna elements. The total undesired noise at the output is denoted as N_T. The receiver makes a binary decision based on the test statistic as

$$\begin{aligned} G(i) \geq 0 &\Rightarrow b_i^1 = 1 \\ G(i) < 0 &\Rightarrow b_i^1 = -1. \end{aligned} \tag{14}$$

V. BER Analysis

In this section, we derive the BER for a DS-UWB system with antenna array. In order to derive the BER, we define the energy of the desired signal at the correlator output and derive the means and variances of the noise and interference terms.

Let the energy of the received monopulse be $E_w = \int_{-\infty}^{\infty} w^2(t)\,dt$. The normalized energy of one data symbol E_{bit} can be calculated as

$$\begin{aligned} E_{\text{bit}} &= \frac{1}{N_s E_w}\int_{-\infty}^{\infty} q_i^2(t)\,dt \\ &= \frac{1}{N_s E_w}\int_{-\infty}^{\infty}\left(\sum_{j=iN_s}^{(i+1)N_s-1} b_i^{(u)} a_j^{(u)} w(t-iT_b-jT_c)\right)^2 dt \\ &= \frac{1}{N_s E_w} N_s \int_{-\infty}^{\infty} w^2(t)\,dt \\ &= \frac{1}{N_s E_w} N_s E_w = 1. \end{aligned} \tag{15}$$

The correlation function of the monopulse is defined as

$$R(\tau) = \int_{-\infty}^{\infty} w(t)w(t-\tau)\,dt. \tag{16}$$

Without loss of generality, we only consider the 0th bit, i.e., $i = 0$ in the remaining analysis for convenience and simplicity of notation. Using (1) and (2), the desired signal at the output

$$\begin{aligned} G_{l_f,m,n}(i) &= \underbrace{\int_{t=iN_sT_c+\tau_{l_f,m,n}}^{(i+1)N_sT_c+\tau^1_{l_f,m,n}} \left[\alpha^1_{l_f,m,n} s^1\left(t-\tau^1_{l_f,m,n}\right)\right] \sum_{j=iN_s}^{(i+1)N_s-1} \alpha^1_{l_f,m,n} a_j^1 w\left(t-jT_c-\tau^1_{l_f,m,n}\right) dt}_{s_{l_f,m,n}} \\ &\quad + \underbrace{Ns_{l_f,m,n} + Nm_{l_f,m,n} + Na_{l_f,m,n}}_{N_{l_f,m,n}} \\ Ns_{l_f,m,n} &= \int_{t=iN_sT_c+\tau^1_{l_f,m,n}}^{(i+1)N_sT_c+\tau^1_{l_f,m,n}} \left(\sum_{\substack{l=0\\ l\neq l_f}}^{L^1_{\text{total}}-1} \alpha^1_{l,m,n} s^1\left(t-\tau^1_{l,m,n}\right)\right) \sum_{j=iN_s}^{(i+1)N_s-1} \alpha^1_{l_f,m,n} a_j^1 w\left(t-jT_c-\tau^1_{l_f,m,n}\right) dt \\ Nm_{l_f,m,n} &= \int_{t=iN_sT_c+\tau^1_{l_f,m,n}}^{(i+1)N_sT_c+\tau^1_{l_f,m,n}} \left(\sum_{u=2}^{N_u}\sum_{l=0}^{L^u_{\text{total}}-1} \alpha^u_{l,m,n} s^u\left(t-\tau^u_{l,m,n}\right)\right) \sum_{j=iN_s}^{(i+1)N_s-1} \alpha^1_{l_f,m,n} a_j^1 w\left(t-jT_c-\tau^1_{l_f,m,n}\right) dt \\ Na_{l_f,m,n} &= \int_{t=iN_sT_c+\tau^1_{l_f,m,n}}^{(i+1)N_sT_c+\tau^1_{l_f,m,n}} \left(\eta'_{m,n}(t)\right) \sum_{j=iN_s}^{(i+1)N_s-1} \alpha^1_{l_f,m,n} a_j^1 w\left(t-jT_c-\tau^1_{l_f,m,n}\right) dt \end{aligned} \tag{12}$$

of the l_fth finger of the (m,n)th element $s_{l_f,m,n}$ in (12) can be written as

$$\begin{aligned} s_{l_f,m,n} &= \int_{t=\tau^1_{l_f,m,n}}^{T_b+\tau^1_{l_f,m,n}} \left[\alpha^1_{l_f,m,n} \sum_{j=0}^{N_s-1} b^1_{i=0} a^1_j w\Big(t-jT_c-\tau^1_{l_f,m,n}\Big)\right] \\ &\quad \times \sum_{j=0}^{N_s-1} \alpha^1_{l_f,m,n} a^1_j w\left(t-jT_c-\tau^1_{l_f,m,n}\right) dt \\ &= \left(\alpha^1_{l_f,m,n}\right)^2 b^1_{i=0} N_s \int_{t=0}^{T_b} w^2(t)dt \\ &= \left(\alpha^1_{l_f,m,n}\right)^2 b^1_{i=0} E_{\text{bit}}. \end{aligned} \tag{17}$$

The total desired signal output s_T in (13) is given by

$$\begin{aligned} s_T &= \sum_{m=0}^{M-1}\sum_{n=0}^{N-1}\sum_{l_f=0}^{L^1_f-1} s_{l_f,m,n} \\ &= \left(\sum_{m=0}^{M-1}\sum_{n=0}^{N-1}\sum_{l_f=0}^{L^1_f-1} \left(\alpha^1_{l_f,m,n}\right)^2\right) b^1_{i=0} E_{\text{bit}}. \end{aligned} \tag{18}$$

The total signal energy in all selected paths from all antenna elements is

$$\begin{aligned} E_s = s^2_T &= \left(\sum_{m=0}^{M-1}\sum_{n=0}^{N-1}\sum_{l_f=0}^{L^1_f-1} \left(\alpha^1_{l_f,m,n}\right)^2\right)^2 \left(b^1_{i=0}\right)^2 E^2_{\text{bit}} \\ &= \left(\sum_{m=0}^{M-1}\sum_{n=0}^{N-1}\sum_{l=0}^{L^1_f-1} \left(\alpha^1_{l_f,m,n}\right)^2\right)^2 E^2_{\text{bit}} \;\; as\left(b^1_{i=0}\right)^2=1. \end{aligned} \tag{19}$$

Assuming that the channel coefficients remain constant during one symbol duration, the AWGN noise term in (12) can be written as

$$\begin{aligned} Na_{l_f,m,n} &= \int_{t=\tau^1_{l_f,m,n}}^{T_b+\tau^1_{l_f,m,n}} \eta'_{m,n}(t) \\ &\quad \times \sum_{j=0}^{N_s-1} \alpha^1_{l_f,m,n} a^1_j w\left(t-jT_c-\tau^1_{l_f,m,n}\right) dt. \end{aligned} \tag{20}$$

The overall AWGN noise at the receiver output can be defined by

$$\begin{aligned} \eta &= \sum_{m=0}^{M-1}\sum_{n=0}^{N-1}\sum_{l_f=0}^{L^1_f-1} Na_{l_f,m,n} \\ &= \sum_{m=0}^{M-1}\sum_{n=0}^{N-1}\sum_{l_f=0}^{L^1_f-1} \left[\int_{t=\tau^1_{l_f,m,n}}^{T_b+\tau^1_{l_f,m,n}} \eta'_{m,n}(t) \sum_{j=0}^{N_s-1} \alpha^1_{l_f,m,n} a^1_j w \right. \\ &\qquad \left. \times \left(t-jT_c-\tau^1_{l_f,m,n}\right) dt\right]. \end{aligned} \tag{21}$$

The mean of this noise term μ_η is zero and is shown as

$$\begin{aligned} \mu_\eta = E[\eta] &= \sum_{m=0}^{M-1}\sum_{n=0}^{N-1}\sum_{l_f=0}^{L^1_f-1} \int_{t=\tau^1_{l_f,m,n}}^{T_b+\tau^1_{l_f,m,n}} E\left[\eta'_{m,n}(t)\right] \\ &\quad \times \sum_{j=0}^{N_s-1} \alpha^1_{l_f,m,n} a^1_j w\left(t-jT_c-\tau^1_{l_f,m,n}\right) dt = 0. \end{aligned} \tag{22}$$

The variance σ^2_η of η is derived in Appendix and is given by

$$\sigma^2_\eta = \frac{N_0}{2} \sum_{m=0}^{M-1}\sum_{n=0}^{N-1}\sum_{l_f=0}^{L^1_f-1} \left(\alpha^1_{l_f,m,n}\right)^2 E_{\text{bit}}. \tag{23}$$

During the 0th bit interval, the MAI contribution $Nm_{l_f,m,n}$ in (12) can be written as

$$\begin{aligned} Nm_{l_f,m,n} &= \sum_{u=2}^{N_u}\sum_{l=0}^{L^u_{\text{total}}-1} \alpha^u_{l,m,n}\alpha^1_{l_f,m,n} \\ &\quad \times \underbrace{\int_{t=\tau^1_{l_f,m,n}}^{T_b+\tau^1_{l_f,m,n}} s^u\left(t-\tau^u_{l,m,n}\right) \sum_{j=0}^{N_s-1} a^1_j w\Big(t-jT_c-\tau^1_{l_f,m,n}\Big) dt}_{I^{u,l}_{l_f,m,n}}. \end{aligned} \tag{24}$$

The term $I^{u,l}_{l_f,m,n}$ in (24) denotes the integration of a function of random variables. Finding a closed-form solution to $I^{u,l}_{l_f,m,n}$ is not feasible. However, we can describe $I^{u,l}_{l_f,m,n}$ in terms of a simplified function of known random variables as described in Appendix. Now, the total MAI at the receiver output can be written as

$$I_{\text{mai}} = \sum_{m=0}^{M-1}\sum_{n=0}^{N-1}\sum_{l_f=0}^{L^1_f-1} Nm_{l_f,m,n}. \tag{25}$$

Substituting (24) in (25), we obtain

$$I_{\text{mai}} = \sum_{m=0}^{M-1}\sum_{n=0}^{N-1}\sum_{l_f=0}^{L^1_f-1}\sum_{u=2}^{N_u}\sum_{l=0}^{L^u_{\text{total}}-1} \alpha^u_{l,m,n}\alpha^1_{l_f,m,n} I^{u,l}_{l_f,m,n}. \tag{26}$$

We assume that I_{mai} is a Gaussian random variable with zero mean and σ^2_{mai} variance. The variance σ^2_{mai} can be written as

$$\begin{aligned} \sigma^2_{\text{mai}} &= \frac{N_s}{T_c} \sum_{m=0}^{M-1}\sum_{n=0}^{N-1}\sum_{l_f=0}^{L^1_f-1}\sum_{u=2}^{N_u}\sum_{l=0}^{L^u_{\text{total}}-1} \left(\alpha^1_{l_f,m,n}\alpha^u_{l,m,n}\right)^2 \\ &\quad \times \int_{-\infty}^{\infty} R^2(x)dx. \end{aligned} \tag{27}$$

The detailed derivation of $\sigma^2_{\rm mai}$ is described in Appendix. Similarly, we can show that SI has zero mean and its variance is

$$\sigma^2_{\rm si} = \frac{N_s}{T_c} \sum_{m=0}^{M-1} \sum_{n=0}^{N-1} \sum_{l_f=0}^{L_f^1-1} \sum_{\substack{l=0 \\ l \neq l_f}}^{L^1_{\rm total}-1} \left(\alpha^1_{l_f,m,n} \alpha^1_{l,m,n} \right)^2 \int_{-\infty}^{\infty} R^2(x) dx. \tag{28}$$

The noise term N_T in (13) is the summation of the total SI ($I_{\rm si}$), MAI ($I_{\rm mai}$), and AWGN (η) at the receiver output that can be rewritten as

$$N_T = \underbrace{\sum_{m=0}^{M-1} \sum_{n=0}^{N-1} \sum_{l_f=0}^{L_f^1-1} Ns_{l_f,m,n}}_{I_{\rm si}} + \underbrace{\sum_{m=0}^{M-1} \sum_{n=0}^{N-1} \sum_{l_f=0}^{L_f^1-1} Nm_{l_f,m,n}}_{I_{\rm mai}} + \underbrace{\sum_{m=0}^{M-1} \sum_{n=0}^{N-1} \sum_{l_f=0}^{L_f^1-1} Na_{l_f,m,n}}_{\eta}. \tag{29}$$

When the number of users is large, we can use the central limit theorem (CLT) to model the $I_{\rm mai}$ by a Gaussian random variable with zero mean and variance $\sigma^2_{\rm mai}$. In UWB, due to its large bandwidth and hence a large number of resolvable paths, the SI $I_{\rm si}$ can also be modeled by a Gaussian random variable with zero mean and variance $\sigma^2_{\rm si}$ using the CLT. As the noise/interference terms $I_{\rm si}$, $I_{\rm mai}$, and η are generated by three independent sources, it is reasonable to assume that they are mutually independent. Hence, N_T is the sum of three mutually independent Gaussian random variables, which in turn is a Gaussian random variable with zero mean and variance $\sigma^2_{\rm total} = \sigma^2_{\rm si} + \sigma^2_{\rm mai} + \sigma^2_{\eta}$.

The probability of error conditioned on a particular instantaneous signal-to-interference-plus-noise ratio (SINR) per bit is given by

$$P_{E/\gamma_b} = Q\left(\sqrt{\frac{E_s}{\sigma^2_{\rm total}}} \right) = Q\left(\sqrt{\frac{E_s}{\sigma^2_{\rm si} + \sigma^2_{\rm mai} + \sigma^2_{\eta}}} \right) \tag{30}$$

where $E_s/\sigma^2_{\rm total}$ is the instantaneous output SINR. For a DS-UWB system under an AWGN channel with single antenna element, (30) reduces to

$$P_E = Q\left(\sqrt{\frac{2E_{\rm bit}}{N_0}} \right). \tag{31}$$

The average bit error probability in the presence of fading is defined as

$$P_E = \int_0^{\infty} P_{E/\gamma_b} P(\gamma_b) d\gamma_b \tag{32}$$

where $P(\gamma_b)$ is the probability density function of instantaneous SNR or SINR at the output of the correlator. The instantaneous SNR/SINR depends on the channel condition. We compute the expectation of the BER under fading using Monte Carlo methods.

TABLE I
PARAMETERS FOR THEORETICAL AND SIMULATION PLOTS OF DS-UWB SYSTEMS

Parameter	**Value**
Location of monopulse center, t_d	0
Width of monopulse, τ_m	$0.7531ns$
Duration of monopulse, τ_w	$\approx 2ns$
Length of Gold sequence	63
Number of chips, N_s	63
Cluster decay factor, Γ	24
Ray decay factor, γ	12
Cluster arrival rate	0.1/ns
Ray arrival rate	0.5/ns
Standard deviation of the cluster lognormal fading term, σ_1	3.3941dB
Standard deviation of the ray lognormal fading term, σ_2	3.3941dB
Total number of multipaths, L_{total}	20

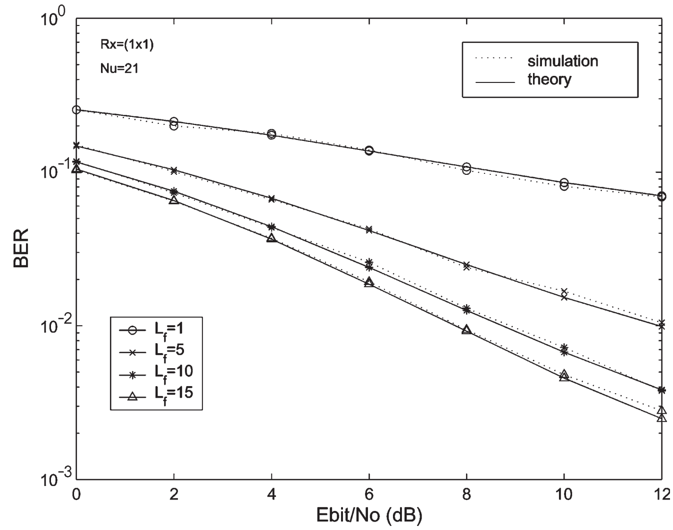

Fig. 2. BER versus $E_{\rm bit}/N_0$ with one receive antenna ($R_x = 1 \times 1$).

VI. Numerical Results

In this section, we present the BER performance and multiple-access capability of the DS-UWB system with different numbers of antenna elements and selected multipaths. Then, we compare the tradeoff between the number of Rake fingers and the size of antenna array. Finally, we study the BER performance of a DS-UWB system with two different array geometries, namely 1) uniform linear array and 2) rectangular array, where each array has the same number of antenna elements. A summary of system parameters is listed in Table I. The average BER $P_E = E[P_{E/\gamma_b}]$ is evaluated using the Monte Carlo method. Using this method, theoretical results are obtained by averaging P_{E/γ_b} over 10000 channel state variables. We use Matlab to obtain the theoretical and simulation results.

Fig. 2 shows both the theoretical and the simulation results of a single receive antenna ($R_x = 1 \times 1$) system for different

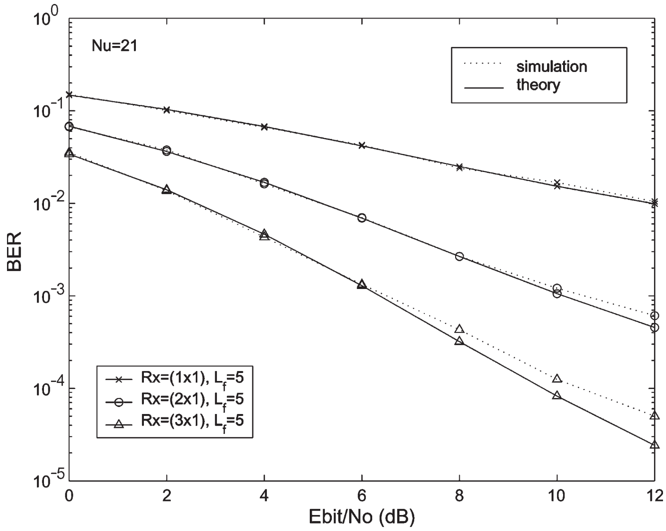

Fig. 3. BER versus $E_{\rm bit}/N_0$ for $R_x = 1\times 1, 2\times 1, 3\times 1$.

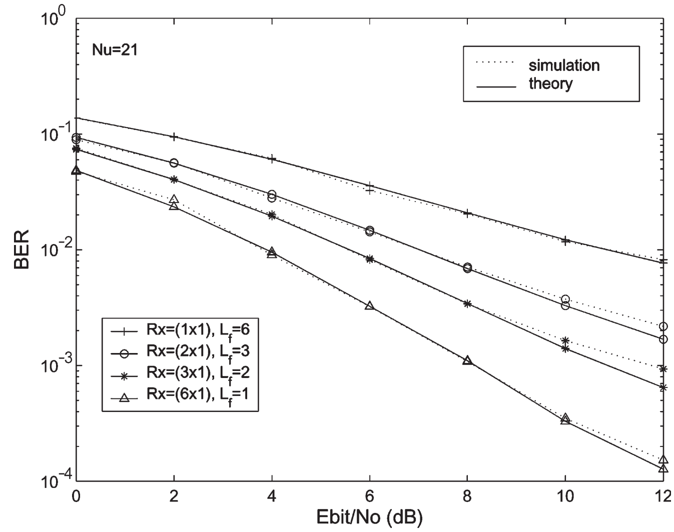

Fig. 5. Tradeoff between the number of Rake fingers and the array size.

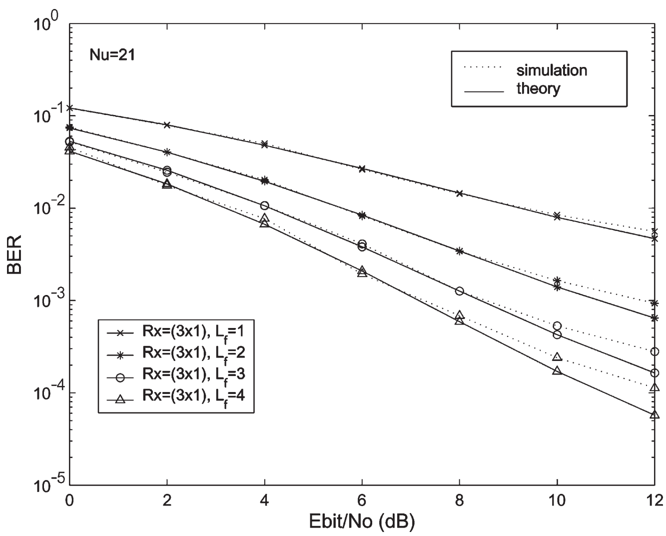

Fig. 4. BER versus $E_{\rm bit}/N_0$ for uniform linear array with $R_x = 3\times 1$.

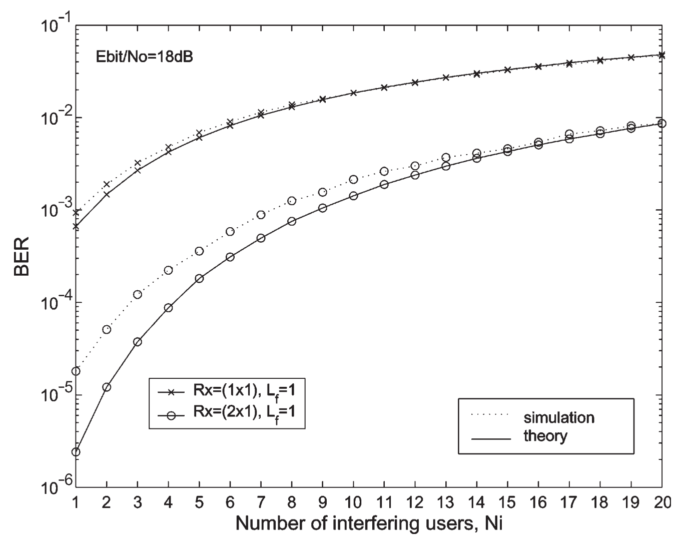

Fig. 6. BER versus number of interfering users N_i.

numbers of selected paths $(L_f = 1, 5, 10, 15)$ when $N_u = 21$. The BER performance improves when more paths are selected and added coherently at the receiver. This is due to an increase in energy captured by the receiver when more paths are selected.

Fig. 3 shows the effect of array size on the BER performance of a DS-UWB system. With $N_u = 21$ and $L_f = 5$, the number of antenna elements is varied from one to three $(R_x = 1\times 1$, 2×1 and $3\times 1)$. From this figure, one can see that the performance of a DS-UWB system can be improved by increasing the number of array elements. This performance improvement comes from the spatial diversity due to multiple antennas.

Fig. 4 shows the effect of the number of selected paths on the BER performance of a DS-UWB system. With $N_u = 21$ and $R_x = 3\times 1$, the BER performance of a system with a uniform linear array is evaluated for different numbers of selected paths $L_f = 1, 2, 3,$ and 4. The results show that the performance of a DS-UWB system improves when the number of selected paths is increased.

The above results show that the performance of a DS-UWB system can be improved by increasing the number of rake fingers and/or the array size. In Fig. 5, we compare the tradeoff between the number of Rake fingers and the antenna array size. In this study, the total number of collected paths by the antenna array is kept at a constant value (six in this simulation), and the BER performance of the system is evaluated for different values of array size. When the array size is changed, the number of selected paths is also changed accordingly such that the total number of collected paths is always equal to six. The results show that a system with higher array size gives better performance. This demonstrates that the performance improvement from spatial diversity is considerably greater than that from the path diversity.

In the next study, we analyze the multiple-access capacity of a DS-UWB system for different antenna array sizes at high $E_{\rm bit}/N_0$. The BER against the number of interfering users $N_i (= N_u - 1)$ is plotted in Fig. 6 for two different array sizes: $R_x = 1\times 1$ and $R_x = 2\times 1$. In this figure, $L_f = 1$

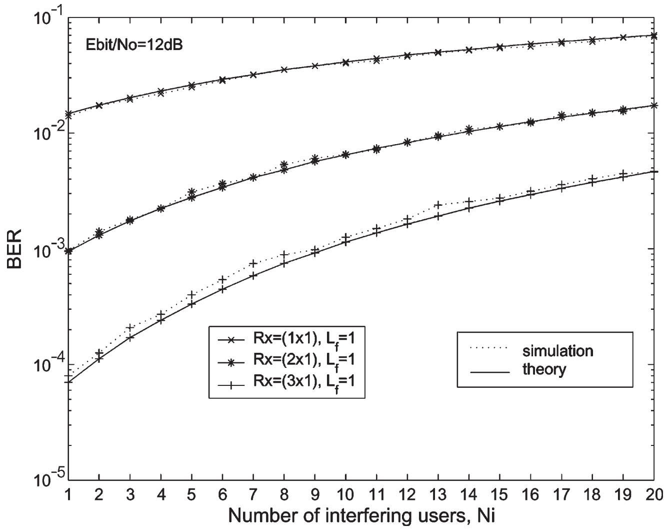

Fig. 7. BER versus number of interfering users at moderate E_{bit}/N_0.

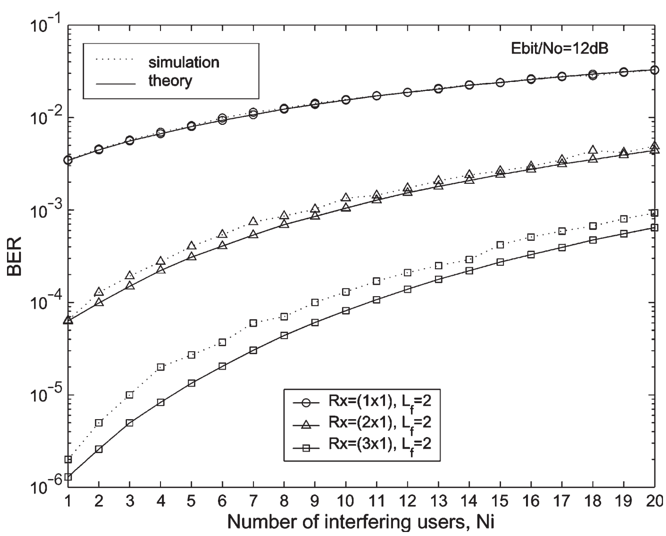

Fig. 8. BER versus number of interfering users with $L_f = 2$.

and $E_{\mathrm{bit}}/N_0 = 18$ dB. The performance degrades when the number of interfering users increases as additional power is required to achieve invariant BER performance. This figure also shows that an antenna array with two elements outperforms the single antenna scheme as expected. An antenna array with MRC allows coherent combining of multipath signal energies and thus effectively mitigating the impact of MAI from other users. This reduction in interference leads to an increase in the multiple-access capacity of the system.

The multiple-access performance at a moderate E_{bit}/N_0 (12 dB) is shown in Figs. 7 and 8, where we use uniform linear arrays with $R_x = 1 \times 1, 2 \times 1,$ and 3×1 elements. Fig. 7 shows the BER as a function of the number of interfering users when $L_f = 1$. This result demonstrates that the system with higher number of array elements has greater tolerance to MAI and can support higher number of simultaneous users. Fig. 8 shows the BER performance as a function of the number of interfering users when $L_f = 2$. Comparing the results in Figs. 7 and 8, one can see that the system with more selected paths supports more users when the array size is fixed.

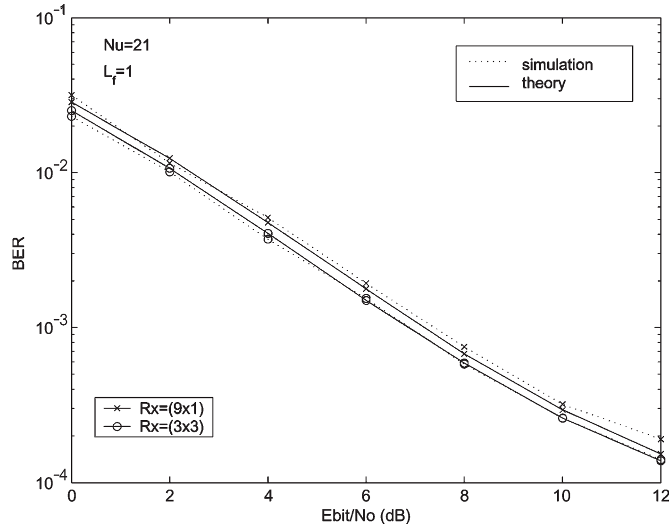

Fig. 9. Comparison between rectangular array and uniform linear array.

In Fig. 9, with $N_u = 21$, we compare the performance of rectangular and uniform linear arrays. In this study, each array has nine elements ($R_x = 9 \times 1$ for the uniform linear array and $R_x = 3 \times 3$ for the rectangular array) and $L_f = 1$. For this simulation, the length of Gold sequence is reduced to 31 and $N_s = 31$ due to excessive computational complexity. The results show that a rectangular array gives better performance than a uniform linear array. This observation can be attributed to the array geometry. The rectangular array is capable of capturing multipath components with shorter propagation delays, and hence the captured energy from the received multipath signals is higher compared to that from the uniform linear array.

VII. Conclusion

In this paper, we evaluated the performance of a DS-UWB multiple-access system with antenna array in dense multipath environments. We showed that an antenna array could be used to exploit the spatial diversity in conjunction with the path diversity provided by the Rake receiver to capture more energy from multipaths in a way to improve the BER performance of the system. The numerical results indicate that the BER performance and the multiple-access capacity of the UWB system can be improved by increasing the number of array size and/or the selected paths. In this paper, we have also shown that the performance improvement from spatial diversity is considerably greater than that from path diversity. Furthermore, we also studied the impact of array geometry on system performance and showed that a rectangular array can capture more energy and thus can offer better performance than a uniform linear array.

In summary, we studied the impact of array geometry, array size (or number of array elements), and number of selected paths on the performance of a DS-UWB system. However, increasing the antenna elements and/or selecting more paths will also increase the system complexity. Therefore, when it comes to system design, a system designer has to choose a suitable array geometry and select appropriate array size (array elements) and number of paths in order to achieve the required performance with minimum increase in system complexity.

APPENDIX

A. Derivation of σ_η^2

Assuming that the noise at the array elements are zero mean independent random variables, the variance of the overall AWGN noise at the receiver output σ_η^2 is defined as

$$\begin{aligned}\sigma_\eta^2 &= E\left[(\eta-\mu_\eta)^2\right] = E[\eta^2], \qquad \mu_\eta = 0\\ &= \sum_{m=0}^{M-1}\sum_{n=0}^{N-1}\sum_{l_f=0}^{L_f^1-1}\int\limits_{\psi=\tau^1_{l_f,m,n}}^{T_b+\tau^1_{l_f,m,n}}\int\limits_{t=\tau^1_{l_f,m,n}}^{T_b+\tau^1_{l_f,m,n}} E\left[\eta'_{m,n}(t)\eta'_{m,n}(\psi)\right]\\ &\quad\times\sum_{j=0}^{N_s-1}\alpha^1_{l_f,m,n}a^1_j w\left(t-jT_c-\tau^1_{l_f,m,n}\right)\\ &\quad\times\sum_{j=0}^{N_s-1}\alpha^1_{l_f,m,n}a^1_j w\left(\psi-jT_c-\tau^1_{l_f,m,n}\right)dt\,d\psi\\ &= \frac{N_0}{2}\sum_{m=0}^{M-1}\sum_{n=0}^{N-1}\sum_{l_f=0}^{L_f^1-1}\left(\alpha^1_{l,m,n}\right)^2\left(\int\limits_{t=0}^{T_b}\sum_{j=0}^{N_s-1}a^1_j w(t-jT_c)dt\right)^2\\ &= \frac{N_0}{2}\sum_{m=0}^{M-1}\sum_{n=0}^{N-1}\sum_{l_f=0}^{L_f^1-1}\left(\alpha^1_{l_f,m,n}\right)^2 E_{\text{bit}}. \end{aligned} \tag{33}$$

B. Evaluation of $\mathrm{I}^{u,l}_{l_f,m,n}$

Fig. 10 illustrates the timing of the local sequence of the desired path (l_f) of the desired user and an interfering signal. In this figure, x is the index for the chip of the desired path, and y is the index for the chip of the interfering signal. The transmission time difference between the selected l_fth path of user 1 and the other interfering paths from the same user or the other users at the (m,n)th element is

$$\begin{aligned}\tau_{l,l_f} &= \tau^u_{l,m,n} - \tau^1_{l_f,m,n}\\ &= \gamma^u_{l,l_f,m,n}T_c + \Delta^u_{l,l_f,m,n}, \qquad u = 1,2,\ldots,N_u\end{aligned} \tag{34}$$

where $\gamma^u_{l,l_f,m,n}$ is the time uncertainty rounded to the nearest integer, and $\Delta^u_{l,l_f,m,n}$ is the error in this rounding process that is uniformly distributed over $[0,T_c]$. Referring to Fig. 10, the integration of $\mathrm{I}^{u,l}_{l_f,m,n}$ in (24) can be written as [19] shown in (35) at the bottom of the page.

By using variable substitution, (35) can be rewritten as shown in (36) at the bottom of the page, which in turn can be rearranged to obtain (37), shown at the bottom of the next page.

In order to simplify $I^{u,l}_{l_f,m,n}$ in (37), we define a set of random variables Z^u_j as [20]

$$Z^u_j = \begin{cases} b^u_{-1}a^u_{j+y-\Delta^u_{l,l_f,m,n}}a^1_{j+x}, & j=0,\ldots,\Delta^u_{l,l_f,m,n}-1\\ b^u_0 a^u_{j+y-\Delta^u_{l,l_f,m,n}}a^1_{j+x}, & j=\Delta^u_{l,l_f,m,n},\ldots,N_s-2\\ b^u_0 a^u_{N_s-1+y-\Delta^u_{l,l_f,m,n}}a^1_{N_s-1+x}, & j=N_s-1\\ b^u_{-1}a^u_{y-\Delta^u_{l,l_f,m,n}-1}a^1_x, & j=N_s. \end{cases} \tag{38}$$

$$\begin{aligned}\mathrm{I}^{u,l}_{l_f,m,n} = &\left[b^u_{-1}\sum_{j=y-\Delta^u_{l,l_f,m,n}}^{y-1}a^u_j a^1_{j+x-y+\Delta^u_{l,l_f,m,n}} + b^u_0\sum_{j=y}^{y+N_s-\Delta^u_{l,l_f,m,n}-1}a^u_j a^1_{j-y+x+\Delta^u_{l,l_f,m,n}}\right]\left(\int_0^{T_c}w(t)w\left(t-\Delta^u_{l,l_f,m,n}\right)dt\right)\\ &+\left[b^u_{-1}\sum_{j=y-\Delta^u_{l,l_f,m,n}-1}^{y-1}a^u_j a^1_{j+x-y+\Delta^u_{l,l_f,m,n}+1} + b^u_0\sum_{j=\Delta^u_{l,l_f,m,n}}^{y+N_s-\Delta^u_{l,l_f,m,n}-2}a^u_j a^1_{j-y+x+\Delta^u_{l,l_f,m,n}+1}\right]\\ &\times\left(\int_0^{T_c}w(t)w\left(T_c-\Delta^u_{l,l_f,m,n}\right)dt\right)\end{aligned} \tag{35}$$

$$\begin{aligned}\mathrm{I}^{u,l}_{l_f,m,n} = &\left[b^u_{-1}\sum_{j=0}^{\Delta^u_{l,l_f,m,n}-1}a^u_{j+y-\Delta^u_{l,l_f,m,n}}a^1_{j+x} + b^u_0\sum_{j=\Delta^u_{l,l_f,m,n}}^{N_s-1}a^u_{j+y-\Delta^u_{l,l_f,m,n}}a^1_{j+x}\right]\left(\int_0^{T_c}w(t)w\left(t-\Delta^u_{l,l_f,m,n}\right)dt\right)\\ &+\left[b^u_{-1}\sum_{j=-1}^{\Delta^u_{l,l_f,m,n}-1}a^u_{j+y-\Delta^u_{l,l_f,m,n}}a^1_{j+x+1} + b^u_0\sum_{j=\Delta^u_{l,l_f,m,n}}^{N_s-2}a^u_{j+y-\Delta^u_{l,l_f,m,n}}a^1_{j+x+1}\right]\left(\int_0^{T_c}w(t)w\left(T_c-\Delta^u_{l,l_f,m,n}\right)dt\right)\end{aligned} \tag{36}$$

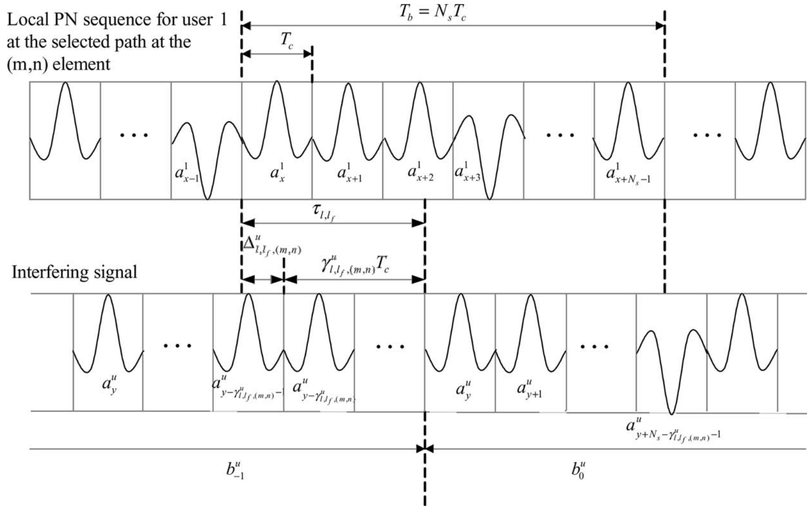

Fig. 10. Timing of the local sequence of the desired path of the desired user with an interfering signal.

The random variables Z_j^u are independent Bernoulli trials and satisfy $\Pr\{Z_j^u = +1\} = \Pr\{Z_j^u = -1\} = 1/2$. By using (38) and the fact that $a_j^1 a_j^1 = 1$, the expression of $I_{l_f,m,n}^{u,l}$ in (37) can be simplified as shown in (39) at the bottom of the page.

Let us define the following four variables:

$$F^u = \sum_{j\in P} Z_j^u, \{P\} \in [0, N_s-2], \quad a^1_{j+x}a^1_{j+x+1} = 1 \tag{40}$$

$$G^u = \sum_{j\in D} Z_j^u, \{D\} \in [0, N_s-2], \quad a^1_{j+x}a^1_{j+x+1} = -1 \tag{41}$$

$$U^u = Z^u_{N_s-1} \tag{42}$$

$$V^u = Z^u_{N_s}. \tag{43}$$

$$\begin{aligned}
\mathrm{I}^{u,l}_{l_f,m,n} = &\left[\sum_{j=0}^{\Delta^u_{l,l_f,m,n}-1} b^u_{-1} a^u_{j+y-\Delta^u_{l,l_f,m,n}} a^1_{j+x} + \sum_{j=\Delta^u_{l,l_f,m,n}}^{N_s-2} b^u_0 a^u_{j+y-\Delta^u_{l,l_f,m,n}} a^1_{j+x} + \underbrace{b^u_0 a^u_{N_s-1+y-\Delta^u_{l,l_f,m,n}} a^1_{N_s-1+x}}_{j=N_s-1}\right]\\
&\times\left(\int_0^{T_c} w(t)w\left(t-\Delta^u_{l,l_f,m,n}\right)dt\right)\\
&+\left[\sum_{j=0}^{\Delta^u_{l,l_f,m,n}-1} b^u_{-1} a^u_{j+y-\Delta^u_{l,l_f,m,n}} a^1_{j+x+1} + \sum_{j=\Delta^u_{l,l_f,m,n}}^{N_s-2} b^u_0 a^u_{j+y-\Delta^u_{l,l_f,m,n}} a^1_{j+x+1} + \underbrace{b^u_{-1} a^u_{y-\Delta^u_{l,l_f,m,n}-1} a^1_{x}}_{j=N_s}\right]\\
&\times\left(\int_0^{T_c} w(t)w\left(T_c-\Delta^u_{l,l_f,m,n}\right)dt\right)
\end{aligned} \tag{37}$$

$$\begin{aligned}
I^{u,l}_{l_f,m,n} = \sum_{j=0}^{N_s 2} Z^u_j &\left(\left[\int_0^{T_c} w(t)w\left(t-\Delta^u_{l,l_f,m,n}\right)dt\right] + a^1_{j+x}a^1_{j+x+1}\left[\int_0^{T_c} w(t)w\left(t-\left(T_c-\Delta^u_{l,l_f,m,n}\right)\right)dt\right]\right)\\
&+Z^u_{N_s-1}\left[\int_0^{T_c} w(t)w\left(t-\Delta^u_{l,l_f,m,n}\right)dt\right] + Z^u_{N_s}\left[\int_0^{T_c} w(t)w\left(t-\left(T_c-\Delta^u_{l,l_f,m,n}\right)\right)dt\right]
\end{aligned} \tag{39}$$

Using (40)–(43), (39) can be rewritten as

$$\begin{aligned} I^{u,l}_{l_f,m,n} = F^u & \left[\int_0^{T_c} w(t) w\left(t - \Delta^u_{l,l_f,m,n}\right) dt \right. \\ & \left. + \int_0^{T_c} w(t) w\left(t - \left(T_c - \Delta^u_{l,l_f,m,n}\right)\right) dt \right] \\ & + G^u \left[\int_0^{T_c} w(t) w\left(t - \Delta^u_{l,l_f,m,n}\right) dt \right. \\ & \left. - \int_0^{T_c} w(t) w\left(t - \left(T_c - \Delta^u_{l,l_f,m,n}\right)\right) dt \right] \\ & + U^u \left[\int_0^{T_c} w(t) w\left(t - \Delta^u_{l,l_f,m,n}\right) dt \right] \\ & + V^u \left[\int_0^{T_c} w(t) w\left(t - \left(T_c - \Delta^u_{l,l_f,m,n}\right)\right) dt \right]. \end{aligned} \tag{44}$$

Now, we explain the probability density functions of F^u, G^u, U^u, and V^u. Denote the number of elements in set $\{P\}$ as p and the number of elements in set $\{D\}$ as d. The probability density functions for F^u and G^u can be written as

$$P_{F^u}(j) = \binom{p}{\frac{j+p}{2}} \left(\frac{1}{2}\right)^p, \quad j = -p, -p+2, \ldots, p-2, p \tag{45}$$

$$P_{G^u}(j) = \binom{d}{\frac{j+d}{2}} \left(\frac{1}{2}\right)^d, \quad j = -d, -d+2, \ldots, d-2, d. \tag{46}$$

The distribution of U^u and V^u can be written as $P_{U^u}(j) = P_{V^u}(j) = 1/2$, where $j = -1, 1$.

C. Derivation of σ^2_{mai}

In (26), we derived an equation for I_{mai}. In this section, we derive an analytical equation for the variance of I_{mai}, σ^2_{mai}. The conditional variance for I_{mai} can be defined as

$$\begin{aligned} & \sigma^2_{\mathrm{mai}|\,\Delta^u_{l_f,l,m,n},d} \\ & = \mathrm{var}\left(I_{\mathrm{mai}} \mid \left\{\Delta^u_{l_f,l,m,n}\right\}, d\right) \\ & = \left[\sum_{m=0}^{M-1} \sum_{n=0}^{N-1} \sum_{l_f=0}^{L^1_f - 1} \sum_{u=2}^{N_u} \sum_{l=0}^{L^u_{\mathrm{total}}-1} \left(\alpha^u_{l,m,n} \alpha^1_{l_f,m,n}\right)^2 \right. \\ & \quad \left. \times E\left[\left(I^{u,l}_{l_f,m,n}\right)^2 \middle| \Delta^u_{l_f,l,m,n}, d \right] \right]. \end{aligned} \tag{47}$$

For convenience, we define the cross correlation of the monopulse as

$$\int_0^{T_c} w(t) w\left(t - \Delta^u_{l,l_f,m,n}\right) dt = \rho_\Delta \tag{48}$$

$$\int_0^{T_c} w(t) w\left(t - \left(T_c - \Delta^u_{l,l_f,m,n}\right)\right) dt = \rho_{T_c - \Delta}. \tag{49}$$

Since the random variables F^u, G^u, U^u, and V^u in (44) are uncorrelated, from (47)–(49), $E[(I^{u,l}_{l_f,m,n})^2 | \Delta^u_{l_f,l,m,n}, d]$ can be written as

$$\begin{aligned} & E\left[\left(I^{u,l}_{l_f,m,n}\right)^2 \middle| \Delta^u_{l_f,l,m,n}, d \right] \\ & = E\left[(F^u)^2 \,|d\right] (\rho_\Delta + \rho_{T_c-\Delta})^2 + E\left[(G^u)^2 \,|d\right] (\rho_\Delta - \rho_{T_c-\Delta})^2 \\ & \quad + E\left[(U^u)^2\right] \rho^2_\Delta + E\left[(V^u)^2\right] \rho^2_{T_c-\Delta}. \end{aligned} \tag{50}$$

The random variables U^u and V^u take a value of -1 or 1 with equal probability; therefore, $E[(U^u)^2] = 1$, $E[(V^u)^2] = 1$. From (40) and (41), p is the number of possible values of j such that $a^1_{j+x} a^1_{j+x+1} = 1$, and d is the number of possible values of j such that $a^1_{j+x} a^1_{j+x+1} = -1$ for $j \in [0, N_s - 2]$. Now, $E[(F^u)^2 | d]$ and $E[(G^u)^2 | d]$ in (50) can be defined as

$$E\left[(F^u)^2 | d\right] = \sum_{x=0}^{p-1} E\left[(F_x)^2\right] = p = N_s - d - 1 \tag{51}$$

$$E\left[(G^u)^2 | d\right] = \sum_{x=0}^{d-1} E\left[(G_x)^2\right] = d. \tag{52}$$

Using $E[(V^u)^2]$, $E[(U^u)^2]$, $E[(F^u)^2 | d]$, and $E[(G^u)^2 | d]$ defined above, (50) can be simplified as

$$\begin{aligned} E\left[\left(I^{u,l}_{l_f,m,n}\right)^2 \middle| \Delta^u_{l_f,l,m,n}, d \right] & = N_s \left(\rho^2_\Delta + 2\rho_\Delta \rho_{T_c-\Delta} + \rho^2_{T_c-\Delta}\right) \\ & \quad - 4d \rho_\Delta \rho_{T_c-\Delta} - 2\rho_\Delta \rho_{T_c-\Delta}. \end{aligned} \tag{53}$$

Assuming random spreading sequences for each user and averaging (53) over d with $E[d] = (N_s - 1)/2$, (53) reduces to

$$\begin{aligned} & E\left[\left(I^{u,l}_{l_f,m,n}\right)^2 \middle| \Delta^u_{l_f,l,m,n} \right] \\ & = N_s \left(\rho^2_\Delta + 2\rho_\Delta \rho_{T_c-\Delta} + \rho^2_{T_c-\Delta}\right) \\ & \quad - 4\left((N_s - 1)/2\right) \rho_\Delta \rho_{T_c-\Delta} - 2\rho_\Delta \rho_{T_c-\Delta} \\ & = N_s \left(\rho^2_\Delta + \rho^2_{T_c-\Delta}\right). \end{aligned} \tag{54}$$

The probability density of $\Delta^u_{l_f,l,m,n}$, $p_\Delta(x)$ is defined as $p_\Delta(x) = T_c^{-1}$, where $-T_c/2 \le x \le T_c/2$. By taking the expectation value of $(I^{u,l}_{l_f,m,n})^2|\Delta^u_{l_f,l,m,n}$ over $\Delta^u_{l_f,l,m,n}$, (54) becomes

$$\begin{aligned} E\left[\left(I^{u,l}_{l_f,m,n}\right)^2\right] &= N_s \int_0^{T_c} \left(\rho^2_\Delta + \rho^2_{T_c-\Delta}\right) \frac{1}{T_c} dx \\ &= \frac{N_s}{T_c} \int_0^{T_c} \left(\rho^2_\Delta + \rho^2_{T_c-\Delta}\right) dx \\ &= \frac{N_s}{T_c} \int_{-\infty}^{\infty} R^2(x) dx. \qquad (55) \end{aligned}$$

Hence, by substituting (55) in (47), σ^2_{mai} can be written as

$$\sigma^2_{\mathrm{mai}} = \frac{N_s}{T_c} \sum_{m=0}^{M-1} \sum_{n=0}^{N-1} \sum_{l_f=0}^{L_f^1-1} \sum_{u=2}^{N_u} \sum_{l=0}^{L^u_{\mathrm{total}}-1} \left(\alpha^1_{l_f,m,n} \alpha^u_{l,m,n}\right)^2 \times \int_{-\infty}^{\infty} R^2(x) dx. \qquad (56)$$

REFERENCES

[1] M. Z. Win and R. A. Scholtz, "Impulse radio: How it works," *IEEE Commun. Lett.*, vol. 2, no. 2, pp. 36–38, Feb. 1998.

[2] ——, "Ultra-wide bandwidth time-hopping spread-spectrum impulse radio for wireless multiple-access communications," *IEEE Trans. Commun.*, vol. 48, no. 4, pp. 679–691, Apr. 2000.

[3] J. R. Foerster, "The performance of a direct-sequence spread ultra-wideband system in the presence of multipath, narrowband interference, and multiuser interference," in *Proc. IEEE Conf. Ultra Wideband Syst. and Technol.*, May 2002, pp. 87–91.

[4] B. M. Sadler and A. Swami, "On the performance of UWB and DS-spread spectrum communications," in *Proc. IEEE Conf. Ultra Wideband Syst. and Technol.*, May 2002, pp. 289–292.

[5] N. Boubaker and K. B. Letaief, "Performance analysis of DS-UWB multiple access under imperfect power control," *IEEE Trans. Commun.*, vol. 52, no. 9, pp. 1459–1463, Sep. 2004.

[6] L. P. B. Christensen, "A low-complexity joint synchronization and detection algorithm for single-band DS-CDMA UWB communications," *EURASIP, J. Applied Signal Process.*, vol. 2005, no. 3, pp. 462–470, 2005.

[7] D. Cassioli, M. Z. Win, F. Vatalaro, and A. F. Molisch, "Performance of low-complexity Rake reception in a realistic UWB channel," in *Proc. IEEE ICC*, May 2002, vol. 2, pp. 763–767.

[8] M. Z. Win and R. A. Scholtz, "On the energy capture of ultrawide bandwidth signals in dense multipath environments," *IEEE Commun. Lett.*, vol. 2, no. 9, pp. 245–247, Sep. 1998.

[9] J. D. Choi and W. E. Stark, "Performance analysis of Rake receivers for ultra-wideband communications with PPM and OOK in multipath channels," in *Proc. IEEE ICC*, Apr. 2002, vol. 3, pp. 1969–1973.

[10] J. S. Thompson, P. M. Grant, and B. Mulgrew, "Smart antenna arrays for CDMA systems," *IEEE Pers. Commun.*, vol. 3, no. 5, pp. 16–25, Oct. 1996.

[11] A. J. Paulraj and C. B. Papadias, "Space–time processing for wireless communications," *IEEE Signal Process. Mag.*, vol. 14, no. 6, pp. 49–83, Nov. 1997.

[12] S. S. Tan, B. Kannan, and A. Nallanathan, "Performance of UWB multiple access impulse radio systems in dense multipath environments with antenna array," in *Proc. IEEE Globecom*, Dec. 2003, vol. 4, pp. 2182–2186.

[13] ——, "Multiple access performance of UWB M-ary impulse radio systems with diversity," in *Proc. Joint UWBST & IWUWBS*, May 2004, pp. 346–350.

[14] M. G. M. Hussain, "Principles of space–time array processing for ultrawide-band impulse radar and radio communications," *IEEE Trans. Veh. Technol.*, vol. 51, no. 3, pp. 393–403, May 2002.

[15] R. J.-M. Cramer, M. Z. Win, and R. A. Scholtz, "Impulse radio multipath characteristics and diversity reception," in *Proc. IEEE ICC*, Jun. 1998, vol. 3, pp. 1650–1654.

[16] A. F. Molisch, J. R. Foerster, and M. Pendergrass, "Channel models for ultra-wideband personal area networks," *IEEE Pers. Commun. Mag.*, vol. 10, no. 6, pp. 14–21, Dec. 2003.

[17] J. R. Foerster, (2003, Feb.). "Channel modeling sub-committee report final," Tech. Rep. IEEE 802.15-02/490. [Online]. Available: http://ieee802.org/15/

[18] A. Saleh and R. Valenzuela, "A statistical model for indoor multipath propagation," *IEEE J. Sel. Areas Commun.*, vol. 5, no. 2, pp. 128–137, Feb. 1987.

[19] T. S. Rappaport, *Wireless Commun.*, 2nd ed. Englewood Cliffs, NJ: Prentice-Hall, 2002.

[20] J. Lehnert and M. Pursley, "Error probabilities for binary direct-sequence spread spectrum communications with random signature sequences," *IEEE Trans. Commun.*, vol. COM-35, no. 1, pp. 87–98, Jan. 1987.

Sheu-Sheu Tan (S'03) received the B.Sc. degree from the National University of Malaysia, Bangi, Selangor, Malaysia, in 2001 and the M.Eng. degree in electrical engineering from the National University of Singapore, Singapore, in 2003.

Her current research interests are ultrawideband communication systems, array signal processing, and wireless communications theory.

Arumugam Nallanathan (S'97–M'00–SM'05) received the B.Sc. degree (with honors) from the University of Peradeniya, Peradeniya, Sri Lanka, in 1991, the C.P.G.S. degree from the University of Cambridge, Cambridge, U.K., in 1994, and the Ph.D. degree from the University of Hong Kong, Hong Kong, in 2000, all in electrical engineering.

He is currently an Assistant Professor in the Department of Electrical and Computer Engineering, National University of Singapore, Singapore. His current research interests are high-speed data transmission over wireless links, orthogonal frequency division multiplexing, ultrawideband communications systems, and wireless communications theory.

Dr. Nallanathan currently serves as a Guest Editor for the EURASIP *Journal on Wireless Communications and Networking* Special issue on Ultra-Wideband Communication Systems—Technology and Applications. He also serves as an Associate Editor for the IEEE TRANSACTIONS ON WIRELESS COMMUNICATIONS, the IEEE TRANSACTIONS ON VEHICULAR TECHNOLOGY, the EURASIP *Journal on Wireless Communications and Networking*, and the *Journal of Wireless Communications and Mobile Computing*.

Balakrishan Kannan (S'97–M'01) received the B.Sc. and B.Eng. degrees from the University of Sydney, Sydney, in 1994 and 1995, respectively, and the Ph.D. degree in electrical engineering from the University of Cambridge, Cambridge, U.K., in 2001.

He was a Scientist for five years with the Institute for Infocomm Research, A-Star, Singapore. He was also an Adjunct Assistant Professor at the National University of Singapore from 2001 until 2005. He is currently a Research Fellow at the University of New South Wales, Sydney. His research interests include array signal processing, multiple-input–multiple-output communication systems, and ultrawideband impulse radio.